Turbulent Natural Convection Inside U-shaped Enclosure

Dr. Khudheyer S. Mushatet
College of Engineering
Thiqar University

Abstract

The turbulent buoyancy induced flow and heat transfer characteristics inside U-shaped enclosure has been numerically documented. Fully elliptic Navier-Stockes and energy equations are solved using control volume based finite volume method with a staggered grid arrangements. A computer program using SIMPLEC algorithm is developed to handle the problem of interest. The effect of Rayleigh number and aspect ratio on the studied parameters are examined. The problem is simulated for Ra up to 1016 and aspect ratio of (0.25, 0.35 and 0.5). The k-ϵ model is engaged with the flow equations to model the turbulence while the wall function method is used to model the regions near the walls. The present results show that the aspect ratio and Ra have a significant effect on the flow and thermal characteristics. The rate of heat transfer is increased with the decrease of aspect ratio and increase with Ra. A multi cellular flow has been obtained at decreasing the aspect ratio for Ra up to 10^{12}.

الخلاصـــــة

في هذا البحث أنجزت دراسة عددية لدراسة خصائص انتقال الحرارة وجريان المائع بالحمل الأضطرابي الحر داخل حيز على شكل حرف-U. تم حل معادلات نافير-ستوكس ذات طبيعة القطع الناقص ومعادلة الطاقة بأستخدام اسلوب حجم التحكم المبنية على طريقة الحجم المحدد وبأعتماد اسلوب الشبكة المتباينة وطور برنامجا حسابيا لنمذجة المشكلة الحالية بالأعتماد على خوارزمية الحل المعتمدة على ربط الضغط بالسرعة. تمت النمذجة الحالية بأستخدام ثلاث قيم من النسب الباعية(0.25,0.35,0.5) بينما وصلت أرقام رايلة الى 1016 . تمت معالجة تأثيرات الأضطراب المرافقة للجريان بأستخدام نموذج الأضطراب(k-ϵ) بينما استخدم اسلوب دالة الجدار لمعالجة المناطق القريبة جدا من الجدران. بينت النتائج الحالية أن لعدد رايلة والنسبة الباعية تأثير واضح على خصائص الجريان وانتقال الحرارة حيث أن معدل انتقال الحرارة يزداد مع نقصان قيمة النسبة الباعية وزيادة عدد رايلة . ايضا أوضحت النتائج أنه تم ملاحظة الجريان متعدد الدوامات عند نقصان قيمة النسبة الباعية ولمدى من أرقام رايلة وصلت الى 10^{12}.

1. Introduction

Turbulent natural convection heat transfer in an enclosed enclosures acquired noticeable interest of the researchers in recent years. The importance of this case arises from the importance of the buoyancy induced flows in multiple engineering applications such as energy transfer in building, double glazing unit, solar collectors and natural circulation in the atmosphere. In other hand, in the increasing development of the new technologies, a complex shaped enclosures have been encountered in a diverse engineering applications including under ground cables, cooling systems of micro-electronic devices and electrical equipments. So additional research is needed to understand the flow behavior and heat transfer in these enclosures. Devahl & Johns[1] and Saitoh[2] investigated the natural convection in differentially heated rectangular cavities. They considered the effect of Ra and aspect ratio on the flow and thermal characteristics. References [3]to [8] reviewed the multiple experimental and computational studies on the laminar and turbulent natural convection heat transfer in the enclosed enclosures. Dol and Hanjalic[9] used a low Reynolds number k-ϵ and second moment closure (SMC) model to the turbulent natural convection heat transfer inside a cubic enclosure. The studied Ra was up to 10^{10}. The k-ϵ model gave a better performance in the regions away from the corners and vice versa. The turbulent buoyancy flow in a 2D enclosure was investigated by Omri and Galanis [10]. They adopted a standard k-ϵ model and three different near wall treatments. The results were validated against experimental results of Tian and karayiannis [11]. Also Betts and Bokhari [12] examined the turbulent natural convection in a tall differentially heated rectangular cavity. They measured experimentally the mean and turbulence quantities of the velocity and temperature inside the cavity.

In the present paper, a computational study is performed to predict the turbulent natural convection inside a U-shaped enclosure as shown in Fig.1. The working fluid was air and Pr is fixed to be 0.72. Three different values of aspect ratios (0.25, 0.35, 0.5) are tested for Ra up to 10^{16}. As shown in Fig1., The enclosure is differentially heated and the left ,bottom and the right walls have higher temperature than the opposite internal walls. Because of symmetry one section of the enclosure has been considered. In the subsequent sections, the results are introduced in the form of isotherm and streamlines contours plots besides to the graphs of local and average Nusselt number variation against the studied parameters.

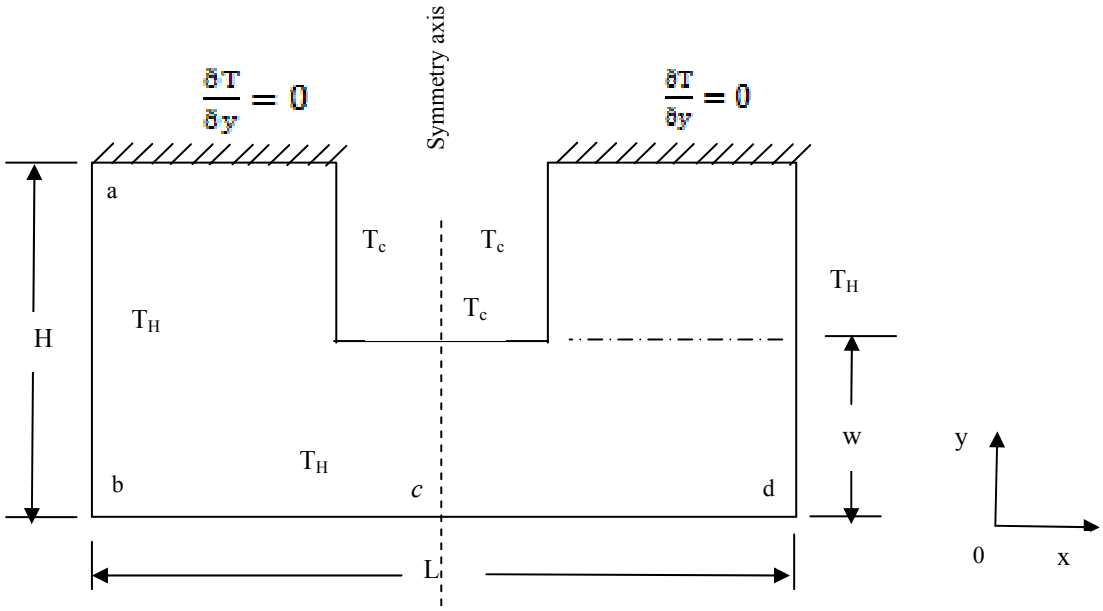

Fig.1 problem definition and coordinates system.

2. Mathematical Formulation

The molecular transport properties of the air are assumed to be constant. The density of air is considered constant except in the buoyancy term of the momentum equation where a linear dependence on temperature is presented. Thus the governing equations associated with a k-ϵ model are introduced as follows[13]:

$$\frac{\partial u}{\partial x}+\frac{\partial v}{\partial y}=0 \qquad \text{.....(1)}$$

$$\rho u\frac{\partial u}{\partial x}+\rho v\frac{\partial u}{\partial y}=-\frac{\partial p}{\partial x}+2\frac{\partial}{\partial x}\left(\mu_{eff}\frac{\partial u}{\partial x}\right)+\frac{\partial}{\partial y}\left(\mu_{eff}\frac{\partial u}{\partial y}\right)+\frac{\partial}{\partial y}\left(\mu_{eff}\frac{\partial v}{\partial x}\right) \qquad \text{.....(2)}$$

$$\rho u\frac{\partial v}{\partial x}+\rho v\frac{\partial v}{\partial y}=-\frac{\partial p}{\partial y}+\frac{\partial}{\partial x}\left(\mu_{eff}\frac{\partial v}{\partial x}\right)+2\frac{\partial}{\partial y}\left(\mu_{eff}\frac{\partial v}{\partial y}\right)+\frac{\partial}{\partial x}\left(\mu_{eff}\frac{\partial u}{\partial y}\right)+\rho g\beta\left(T-T_0\right) \qquad \text{...(3)}$$

$$\rho u\frac{\partial T}{\partial x}+\rho v\frac{\partial T}{\partial y}=\frac{\partial}{\partial x}\left(\Gamma_{eff}\frac{\partial T}{\partial x}\right)+\frac{\partial}{\partial y}\left(\Gamma_{eff}\frac{\partial T}{\partial y}\right) \qquad \text{.....(4)}$$

$$\mu_{eff}=\mu+\mu_t, T_0=\left(T_C+T_H\right)/2,\ \beta=1/T_0 \qquad \text{... ....(5)}$$

$$\Gamma_{eff,T}=\frac{\mu}{\mathrm{Pr}}+\frac{\mu_t}{\mathrm{Pr}} \qquad \text{.....(6)}$$

The stream function ψ is obtain by solving the following Poisson equation with the boundary condition ψ = 0 at all the solid walls.

$$\frac{\partial^2\psi}{\partial^2 x}+\frac{\partial^2\psi}{\partial^2 y}=\frac{\partial u}{\partial y}+\frac{\partial v}{\partial x} \qquad \text{.....(7)}$$

The turbulent kinetic energy and the rate of its dissipation for two dimensional buoyancy turbulent flow has been introduced including additional term of kinetic energy generation by buoyancy [14].

$$\rho u\frac{\partial k}{\partial x}+\rho v\frac{\partial k}{\partial y}=\frac{\partial}{\partial x}\left(\Gamma_{eff,k}\frac{\partial k}{\partial x}\right)+\frac{\partial}{\partial y}\left(\Gamma_{eff,k}\frac{\partial k}{\partial y}\right)+G+G_{\mathbf{B}}-\rho\varepsilon \qquad \text{.....(8)}$$

$$\rho u\frac{\partial \varepsilon}{\partial x}+\rho v\frac{\partial \varepsilon}{\partial y}=\frac{\partial}{\partial x}\left(\Gamma_{eff,\varepsilon}\frac{\partial \varepsilon}{\partial x}\right)+\frac{\partial}{\partial y}\left(\Gamma_{eff,\varepsilon}\frac{\partial \varepsilon}{\partial y}\right)+C_{1\varepsilon}\frac{\varepsilon}{k}(G+G_B)-C_{2\varepsilon}\frac{\varepsilon^2}{k} \quad (9)$$

where

$$G=\nu_t\left[2\left(\frac{\partial u}{\partial x}\right)+2\left(\frac{\partial v}{\partial y}\right)+\left(\frac{\partial u}{\partial y}+\frac{\partial v}{\partial x}\right)\right] \qquad \text{.....(10)}$$

$$\Gamma_{eff,k}=\mu+\frac{\mu_t}{\sigma_k},\quad \Gamma_{eff,\varepsilon}=\mu+\frac{\mu_t}{\sigma_t},\quad \Gamma_t=\frac{\mu_t}{\sigma_t},\quad G_B=g\beta\Gamma_t\frac{\partial T}{\partial y} \qquad \text{...(11)}$$

the eddy dynamic viscosity is obtained by the Prandtl-Kolmogorov hypothesis

$$\nu_T=C_\mu\frac{K^2}{\varepsilon} \qquad \text{.....(12)}$$

the model coefficients are (σ_k ;σ_ϵ ; $C_{1\epsilon}$; $C_{2\epsilon}$; $C\mu$) = (1.0 , 1.3 , 1.44 , 1.92, 0.09) respectively [13]

2-1 Boundary conditions.

The wall function approach [15] is incorporated to model the near wall regions. In order to solve the mathematical model, the following boundary conditions are introduced.

- At the walls: $u=v=k=0.$ and $\frac{\partial\varepsilon}{\partial n}=0.$, n is a unit normal vector.
- At the symmetry axis: $\frac{\partial\phi}{\partial n}=0.$
- The local Nusselt number on the vertical hot wall is $Nu_y=\frac{\partial\Phi}{\partial X}=\frac{\partial T}{\partial x}\frac{H}{T_H-T_C}$

- The local Nusselt number on the horizontal hot wall is $Nu_x = \frac{\partial \Phi}{\partial Y} = \frac{\partial T}{\partial y}\frac{H}{T_H - T_C}$
- The Nu_{av} on the hot walls can be expressed as $\frac{1}{abc}\left[\int_0^1 Nu_x dy + \int_0^1 Nu_y dx\right]$

3. Numerical method

The coupled elliptic governing partial differential equations associated with the turbulence quantities are discretized using the finite volume method. This gives a system of algebraic equations. The solution of these equations is accomplished through a semi-implicit line by line Guass elimination scheme. Non uniform grids in all directions are adopted[16]. A computer program is developed to get the results using the pressure velocity coupling (SIMPLEC algorithm)[15]. Due to this inherent strong coupling and non-linearity in these equations, relaxation factors are needed to ensure the convergence. The relaxation factors used for velocity components, pressure, energy and turbulence quantities are 0.4, 0.5, 0.45, 0.7 respectively. These relaxation factors have been adjusted for each case studied in order to accelerate the convergence. The adopted non-uniform grids are finer near the solid walls where steep gradients of the dependent variable are more important. In general the computational grids are staggered for vector variables and not staggered for the scalar one. For $Ra \le 10^{10}$, the number of the used grids is 31×31 and for $10^{12} \le Ra$ is 61×61. The following criterion should be achieved to get the convergence for all the considered dependent variables.

$$\text{Max}\left|\phi^k(i,j) - \phi^{k-1}(i,j)\right| \le 10^{-5}.$$

4. Results and Discussion

A computational study has been conducted to investigate the turbulent natural convection inside U-shaped enclosure for different aspect ratios and Ra.

The effect of Rayleigh number (Ra = 10^8, 10^{10}, 10^{12}, 10^{14}, 10^{16}) on stream function distribution for A = 0.5 is shown in Fig.2. As the Figure shows, there is a counter rotating cell when Ra = 10^8 . This cell is close to the vertical part of the enclosure rather than the horizontal one. When Ra increase, the size and location of this cell is changed. Also it can be seen that the cell is elongated at High Rayleigh numbers(10^{12}, 10^{14}, 10^{16}). besides, the position of this counter rotating cell is to be closure to the left bottom corner at high Rayleigh numbers. It is observed that there is a secondary flow just behind the right corner. This is confirmed at Figure 5 where the flow is detached from the right corner forming a small re-circulating zone. When the aspect ratio is decreased to 0.35, a multi cellular flow is observed. This situation can be seen in Fig.3. At Ra = 10^8 , there is three counter rotating cells one at the

vertical part and the remaining at the horizontal part. However, the counter rotating cell at the upper part is larger. This is confirmed at Fig.5.b. It is evident that the hot fluid rises along the left hot wall and then deflects along the upper wall forming a re-circulating flow in the two parts of the enclosure. There is a semi-stagnant re-circulating zones and there is no small re-circulating secondary flows near the symmetry axis. When Ra increase to 10^{10} , the three re-circulating vortices decomposes to two recalculating vortices with a larger size. At Ra = 10^{12}, the resulting two re-circulating vortices are elongated and fill nearly a large zone compared with the mentioned two case, Also there is a secondary re-circulating flow just behind the upper corner. This confirmed through Fig.5.e. This elongation is enhanced at Ra = 10^{14} but at Ra = 10^{16}, the two elongated vortices are changed to one elongated vorticity. The stream function distribution for A =0.25 at the considered Ra is exhibited at Fig.4. It can be seen that the multi cellular flow is extended to Ra up to Ra = 10^{12} compared with the previous cases (A=0.25 and A=0.35). However at Ra = 10^{12}, one of the formed counter rotating vortices has a small size and located at the right corner. The size and position of the resulting vortices are different from the previous cases up to 10^{12}. At Ra = 10^{14} to Ra = 10^{16}, the same general behavior is found compared with the other studied cases because when the aspect ratio decrease, the flow hits the upper wall faster. This confirmed through Fig.5. c. and f. where the resulting flow behavior is demonstrated. As Fig.5. shows, at Ra = 10^{12}, the detached re-circulating flow has large and strong zone compared with the previous studied cases. Also it can be seen from Fig.5(a,b,c) at Ra = 10^{8} , the aspect ratio has a significant effect on the flow behavior. This situation is extended to (d, e, f) at Ra = 10^{12}. and this dominant for all the studied Ra. The temperature distribution for different Ra and A = 0.5 is depicted in Fig.6. As the Figure shows at Ra = 10^{8}, the heat is transferred from hot walls to the cold one through a working fluid(air) by convection. The hot re-circulating flow hits the upper portion of the enclosure. The resulting thermo-convective motion is slow and the left corner has high temperature. This confirmed at Fig.12 for Nusselt number variation along the hot wall. When Ra increase, the heat begins to penetrating to the second part of the enclosure because the increase in Ra increase the buoyancy force and that leads to increase the rate of heat transfer. This can be demonstrated at Fig.9. (a) and (b). The lower left corner exhibits low values of Nu and hence low heat transfer. The local Nusselt number increase with the increase of Ra. However the position of maximum and minimum values of Nu is changed with Ra. Fig.7. shows the temperature distribution for different Ra and A= 0.35. It is evident that the thermo-convective currents are increased, consequently, the rate of heat transfer is increased. Also the rate of heat transfer is increased with the increase of Ra.It can be seen that for 10^{8} and at the lower part of the second portion of the enclosure, there is a faster motion of the fluid to the opposite upper part. The heat transfer is significantly increased with the increase of Ra. This behavior is extended to A=0.25 where higher rate of heat transfer is obtained because when the aspect ratio (A) decrease, the hot fluid hits opposite side faster and then reattached and consequently increase the exchange of heat transfer. The average Nusselt number variation with Ra for the considered aspect ratios is depicted in Fig.10. It can be seen that the Nuav is

linearly increased with the increase of the Ra up to 10^{12} and the aspect ratio has a little effect. At Ra= 10^{12} to Ra= 10^{16}, the Nuav is increased with the increase of Ra and the aspect ratio (A) has a large effect. The variation of Nuav with aspect ratio(A) is shown in fig.11 for different Ra. It can be seen that the Nuav is increased with the decrease of aspect ratio for every specified Ra because the smaller aspect ratio permits speedy exchange of heat transfer. The comparison of Nu variation of the vertical hot wall for the considered aspect ratios is described in Fig.12. As it is mentioned, the local Nusselt number increases with decreasing the aspect ratio at Ra = 10^8 , for Ra > 10^8, this situation is the same, but at upper left hot wall there is some deviation. Also Fig.13 shows the variation of Nu on the horizontal hot wall for different values of aspect ratios at Ra = 10^8 and Ra = 10^{12}. In (a), one can be seen that the position of higher and lower values of Nu is changed with the aspect ratio variation. This is a dominant for all the studied cases as shown in (b). The validation of the present code is completed through testing the code with the problem of turbulent natural convection in a square enclosure and then compare the results with published one as shown in fig.14. It can be seen that there is a good agreement has been obtained.

5. Conclusions

Two dimension turbulent buoyancy induced flow inside U-shaped enclosure has been numerically reported. From the presented results, the following remarks can be summarized.

- The rate of heat transfer is enhanced with decreasing the value of aspect ratio.
- The lower values of aspect ratio show a counter rotating multi cellular flow pattern and the higher values show a unicellular one.
- The rate of heat transfer is increased with the increase of Rayleigh number.
- For all the considered aspect ratios, the location and positions of counter rotating cells depends on the values of Ra.
- The left hot corner has a lower values of local Nusselt number and hence a lower heat transfer.
- The average heat transfer is increased with the decrease of aspect ratio.
- The position of maximum and minimum values of Nu along vertical and horizontal hot walls is shifted depending of the values of Ra and A.

Nomenclature

A	aspect ratio (w/H), -
G	generation term, kg/m.sec^3
G_B	generation term by buoyancy, kg/sec^2
H	height of the enclosure, m
k	turbulent kinetic energy, m^2/s^2
L	length of the enclosure, m
Nu	local Nusselt number, -
Nuav	average Nusselt number, -
Pr	Prandtl number, -
Ra	Rayleigh number $\left(\frac{g\beta H^3(T_h - T_c}{\alpha\mu}\right)$,-
w	the distance between two walls, m
T_C	cold wall temperature, Ċ
T_H	hot wall temperature, Ċ
X,Y	dimensionless Cartesian coordinates (x, y)/H, -

Greak symbols

ϵ	turbulance dissipation rate, m^2/s^3
μ	dynamic viscosity, N.s/m^2
μ_t	turbulent viscosity, N.s/m^2
ν_t	eddy dynamic viscosity, m^2/s
μ_{eff}	effective turbulent viscosity, N.s/m^2
Γ_{eff}	effective exchange coefficient, kg/m.s
σ_k ;σ_ϵ	turbulent schmidt numbers, -
ϕ	constant property, -

6. Reference

1. Devahl Davis and Johns, ***" Natural convection in a square cavity"***, Int. J. of Numerical Methods, 1983
2. Saitoh, Hirosek, k., ***" High accuracy benchmark solutions to natural convection in a square cavity***, J. of Computers and Fluids, 1989.
3. Hart,E.J., ***"Stability of the flow in a differentially heated inclined box"***, J. Fluid Mech.,1971.

4. Osttrach, S., ***" Natural convection in enclosure"***, J. Heat Transfer Trans., ASME, 1988.
5. Ganzarolli, M.M, Milane Z, L.F., ***" Natural convection in rectangular enclosures heated from below and symmetrically cooled from the sides",*** Int. J. Heat and Mass Transfer, 1995.
6. Kuyper, R.A, Van Der Meer, C.J., Henkes, R.A***.," Numerical study of laminar and turbulent natural convection in an inclined square cavity***, Int.J. Heat mass Transfer,36,1993.
7. Markatos, N.C., Pericleous, K.A., ***" Laminar and turbulent natural convection in an enclosed cavity",*** Int. J. Heat Mass Transfer, 1984
8. Lankhorst, A.M., Henkes, Hoogendoorn, C.J.,***'' Natural convection in cavities at high Rayleigh numbers"***, second UK national conference on heat transfer, university of Strathclycle, Glasgow, 1991
9. Dol, H.S., Hanjalic, K., ***" Computational study of turbulent natural convection in a sided-heated near cubic enclosure at high Rayleigh number"***, Int. J Heat and Mass Transfer, vol.44., 2001.
10. Omri, M., Galannis, N***.," Numerical analysis of turbulent natural convection in a cavity"***, Heat Mass Transfer, Vol.4., 2003.
11. Tain, Y.s., Karayiannis, t.G., ***" Low turbulence Natural Convection in an air filled square cavity"***, Int. J. Heat Mass Transfer, vol.43, 2000.
12. Betts, P.l., Bkhari, I.H., ***" Experimental and turbulent natural convection in an enclosed tall cavity",*** Int. J. Heat and Fluid Flow, vol.21,2000, PP.,675-683.
13. Jones, W.P., Lunder, B.E., ***The prediction of laminarization with a two equation model of turbulence"***, J. Heat and Mass transfer, 1972.

14. Awbi, H.B., ***" Ventilation of Building",*** E. and FN Spon, London, 1995.

15. Versteege, H. and Meer, W***." An introduction of computational fluid dynamics"***, Hemisophere Publishing Corporation, United State of America, 1995.

16. John, A., Anderson***," Computational Fluid Dynamics***, the basics with applications, 1995.

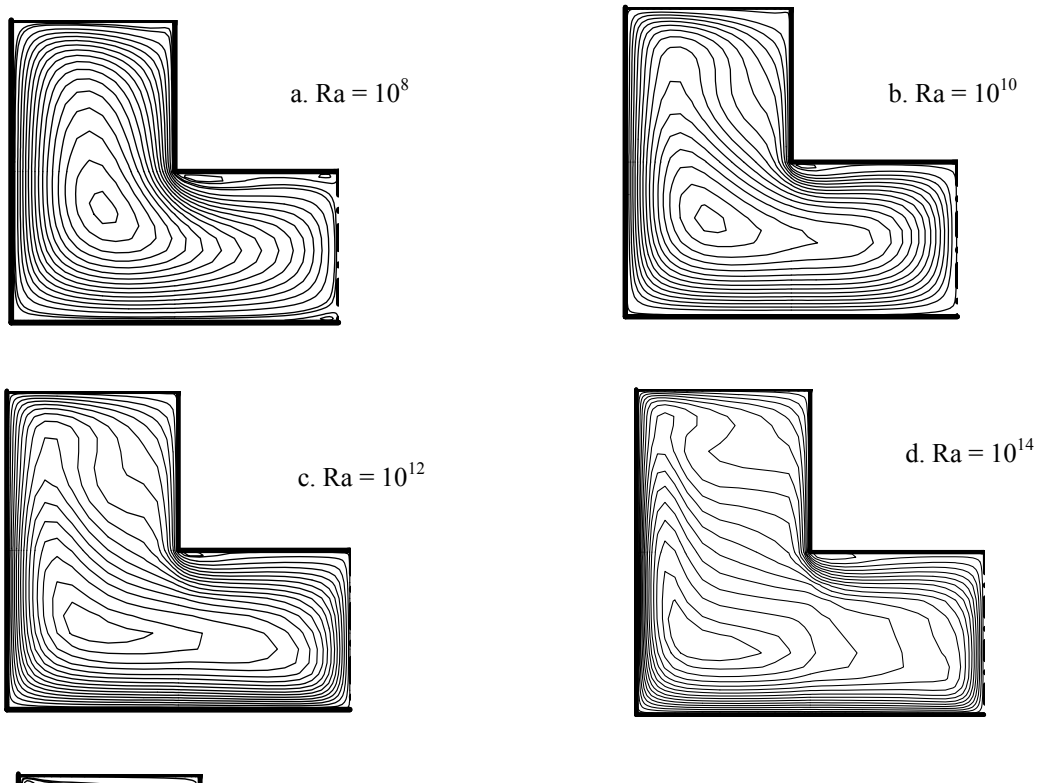

Fig.2. stream function distribution for A= 0.5

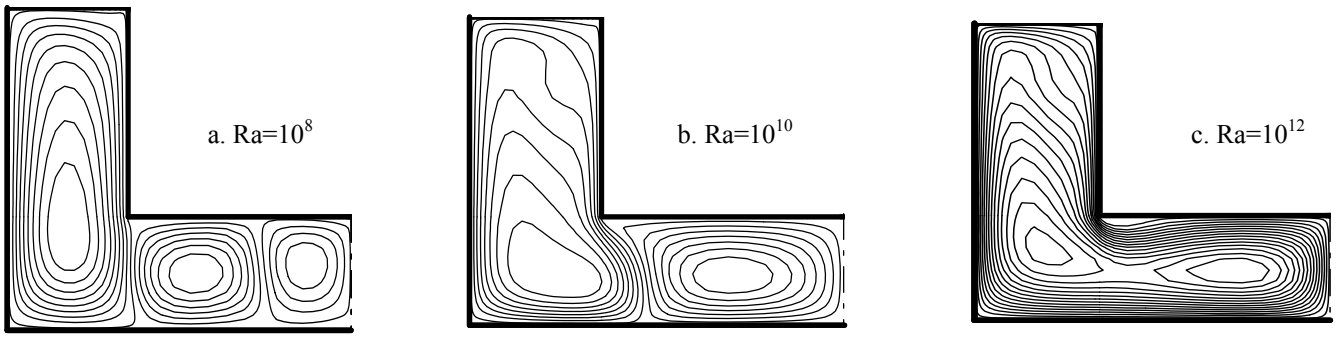

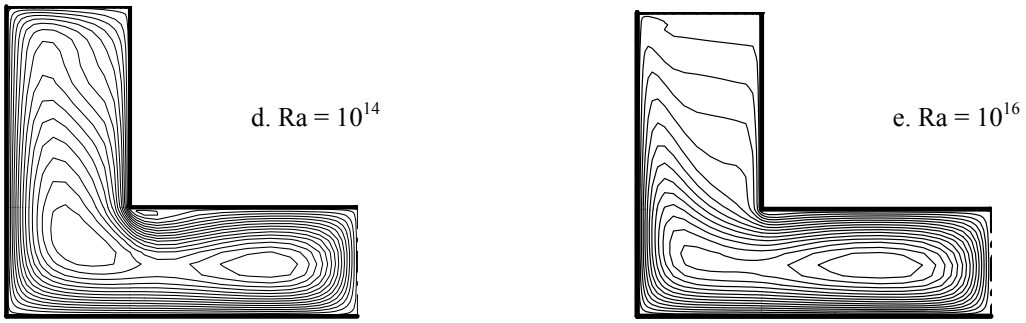

Fig.3. stream function distribution for A= 0.35

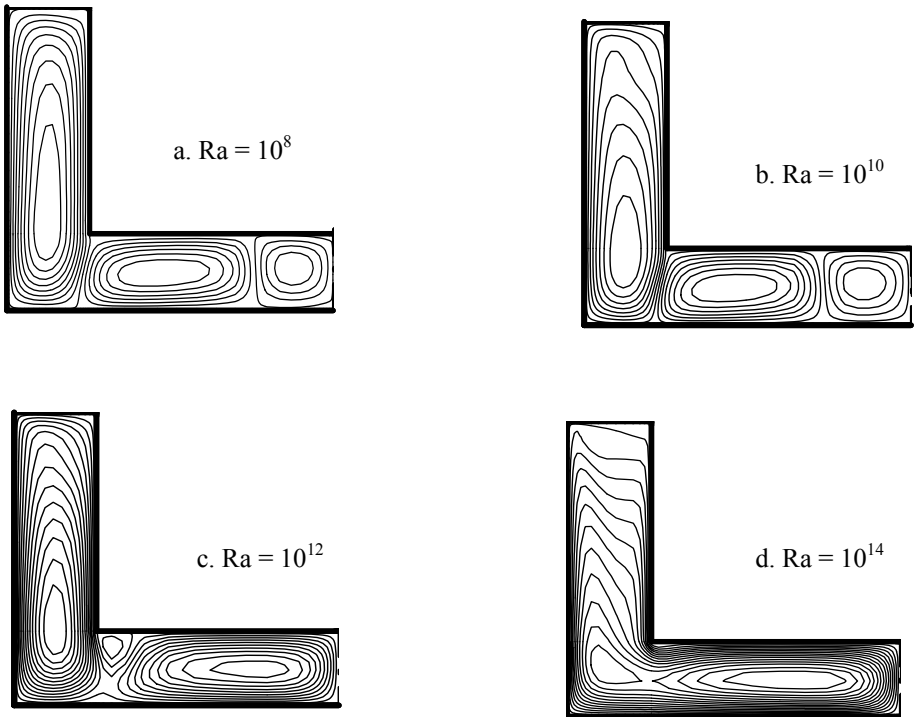

Fig.4. stream function distribution for A= 0.25

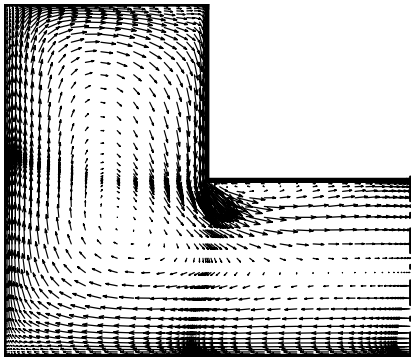

a. A=0.5, Ra=10E8

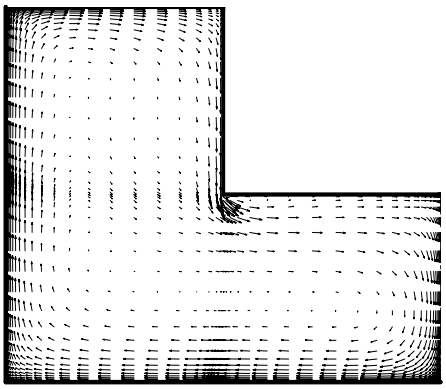

d. A=0.5, Ra=10E12

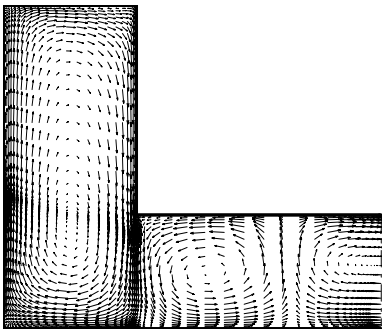

b. A=0.35, Ra=10E8

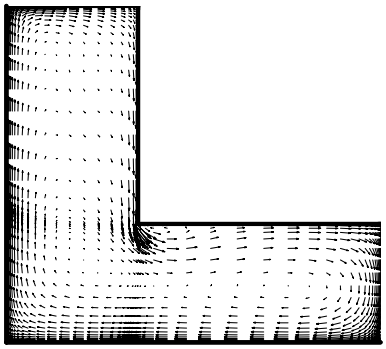

e. A=0.35, Ra=10E12

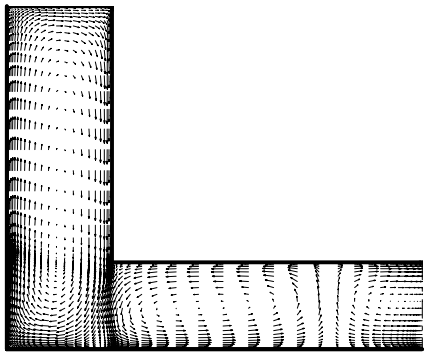

c. A=0.25, Ra=10E8

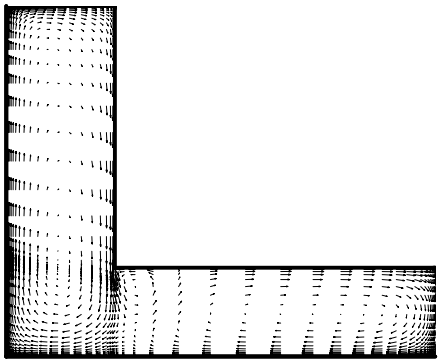

f. A=0.25, Ra=10E12

Fig.5 effect of aspect ratio on the computed velocity vectors

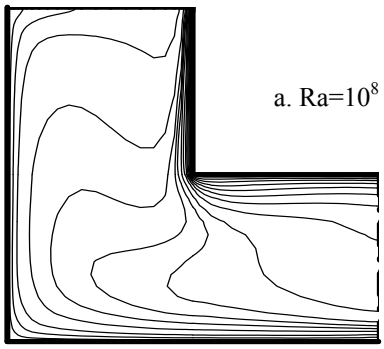

a. Ra=10^8

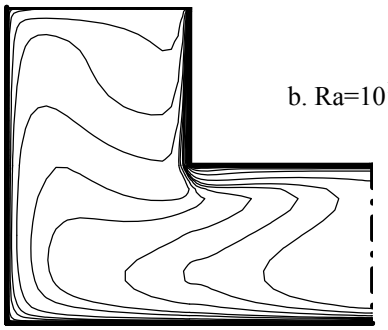

b. Ra=10^{10}

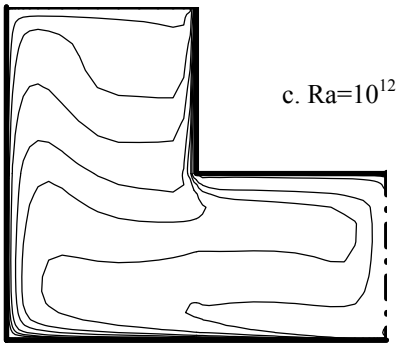

c. Ra=10^{12}

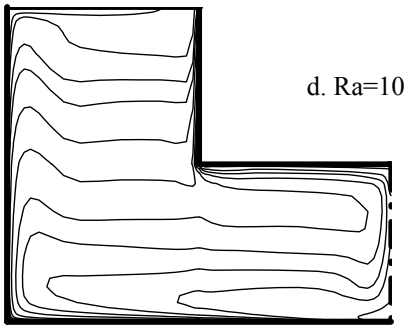

d. Ra=10^{14}

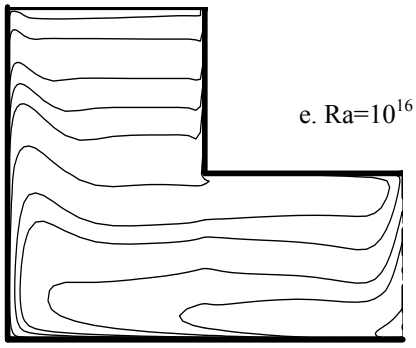

e. Ra=10^{16}

Fig6. isotherm contours for A = 0.5

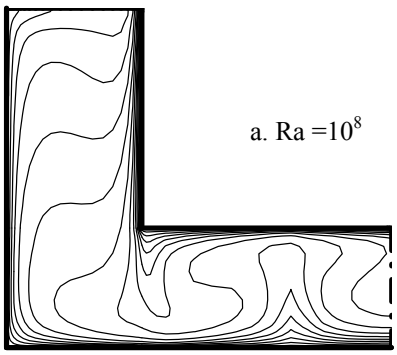

a. Ra =10^8

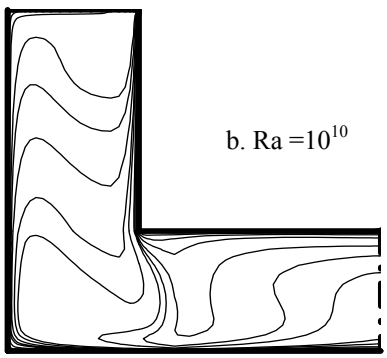

b. Ra =10^{10}

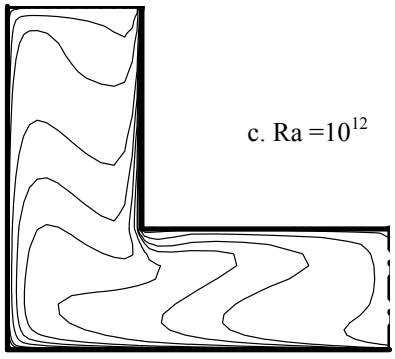

c. Ra =10^{12}

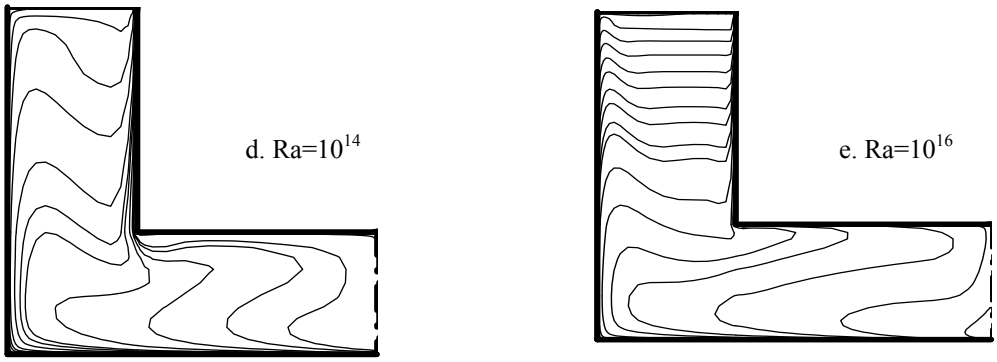

Fig.7. isotherm contours for A = 0.35

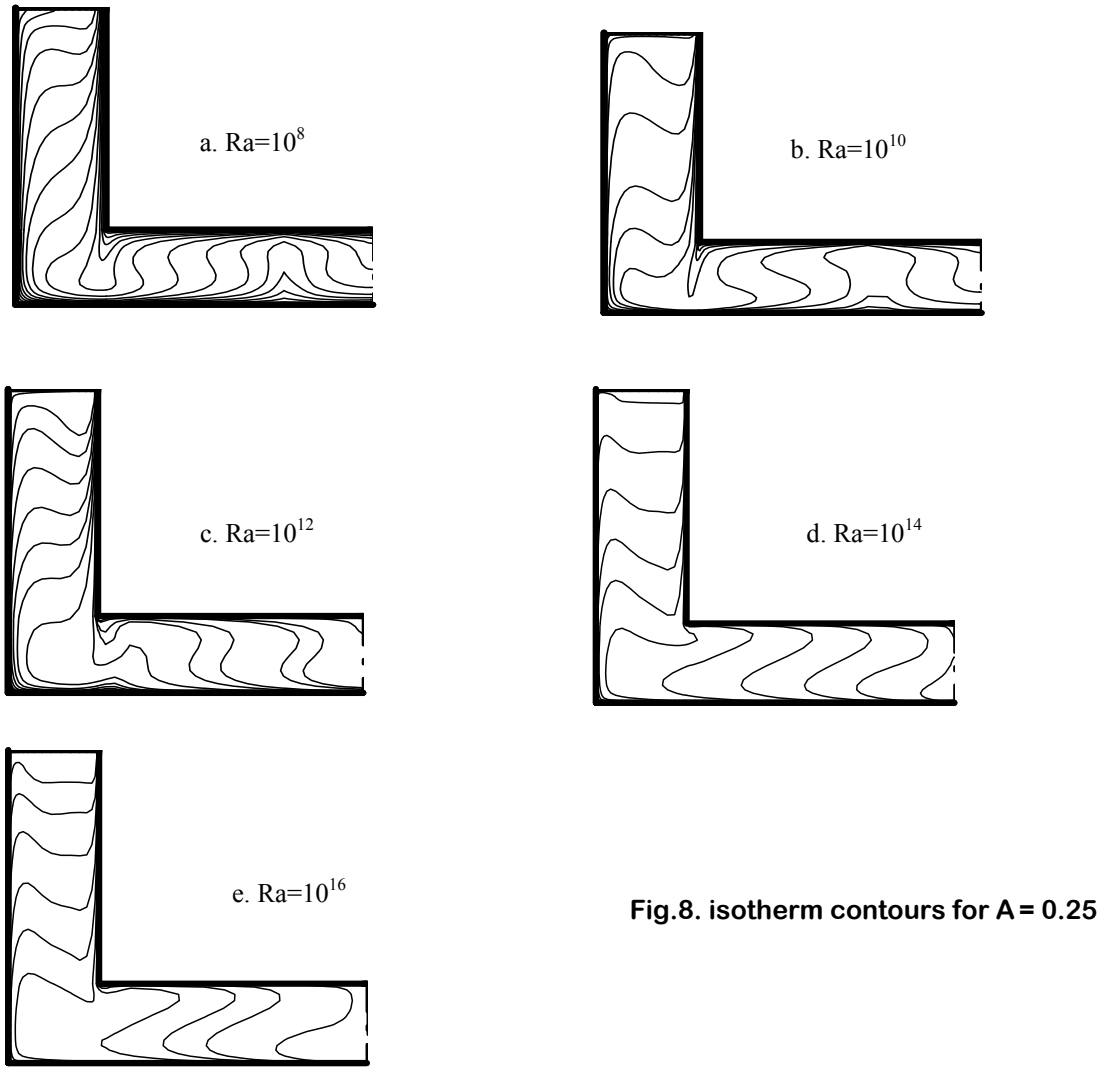

Fig.8. isotherm contours for A = 0.25

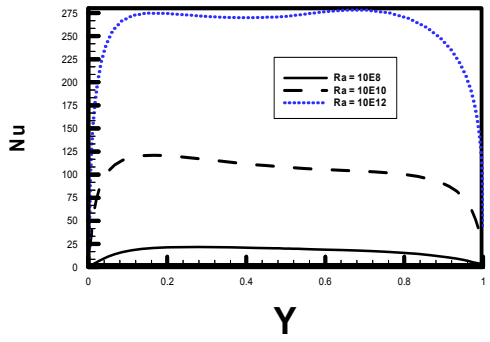

a. A=0.5

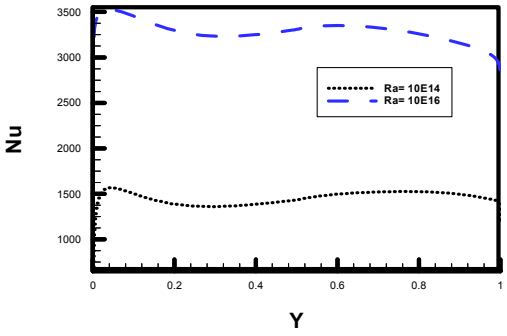

b. A=0.5

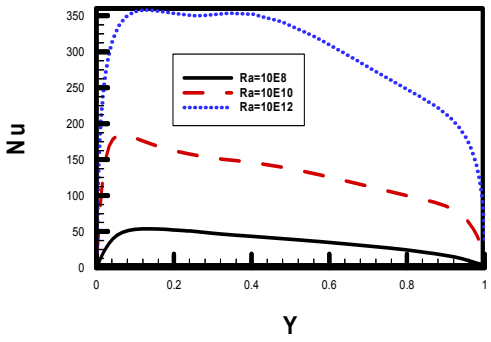

c. A=0.25

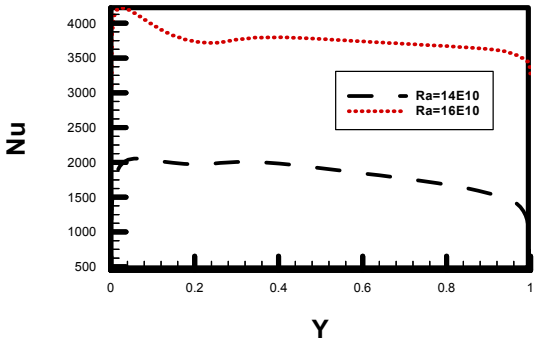

d. A=0.25

Fig.9 variation of local Nusselt number on the vertical hot wall for different Ra

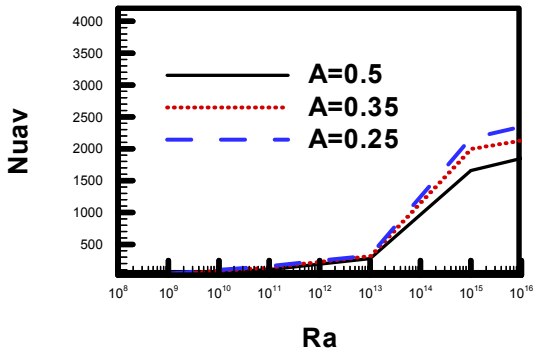

Fig.10 effect of Ra on average Nu distribution at different values of aspect ratio

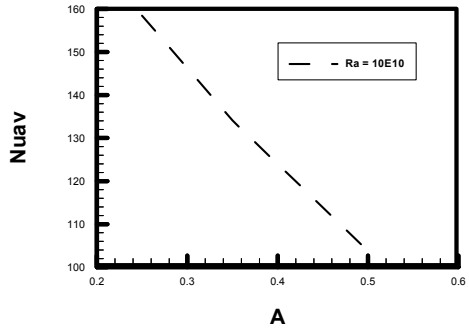

a

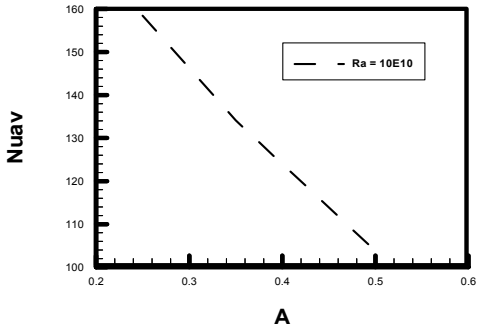

b

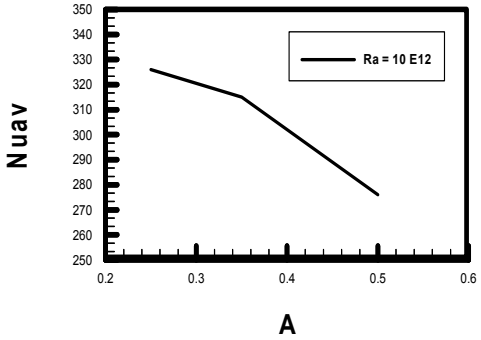

c

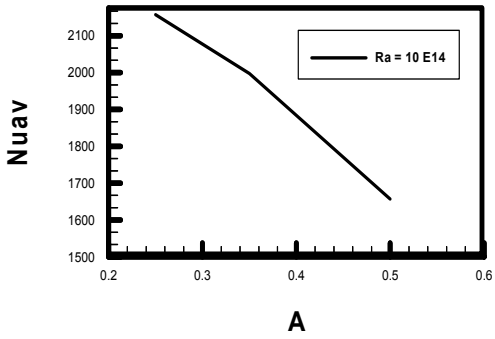

d

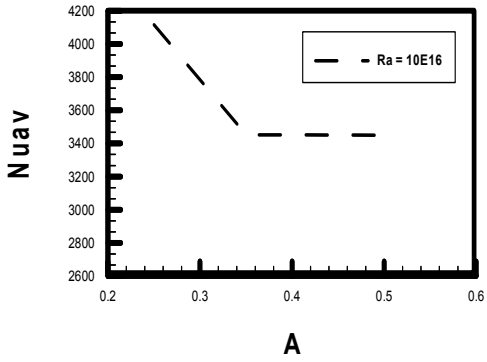

e

Fig.11 variation of Nuav with A for different Ra

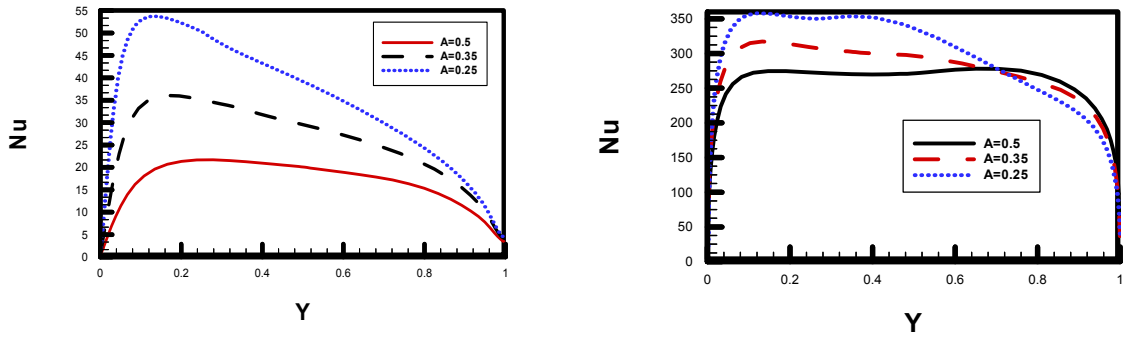

a. Ra = 10E8 b. Ra = 10E12

Fig.12 comparison of the Nu at the vertical hot wall for the considered aspect ratios

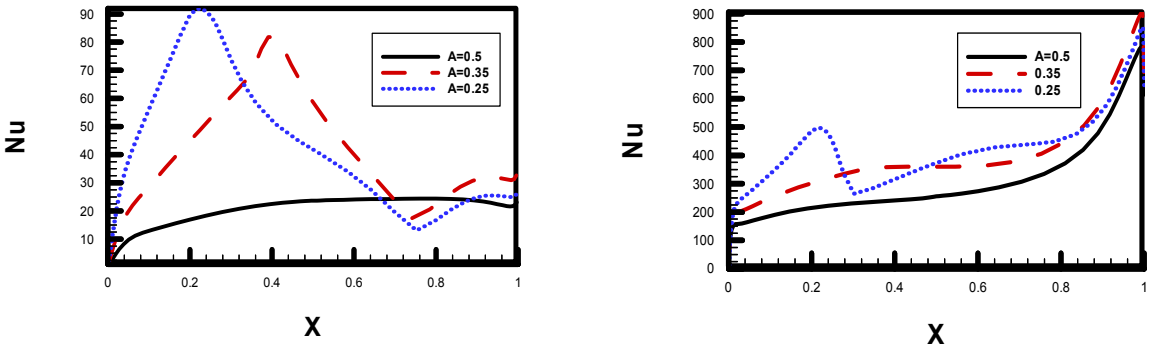

a. Ra = 10E8 b. Ra = 10E12

Fig. 13 comparison of the Nu at the horizontal hot wall for the considered aspect ratios

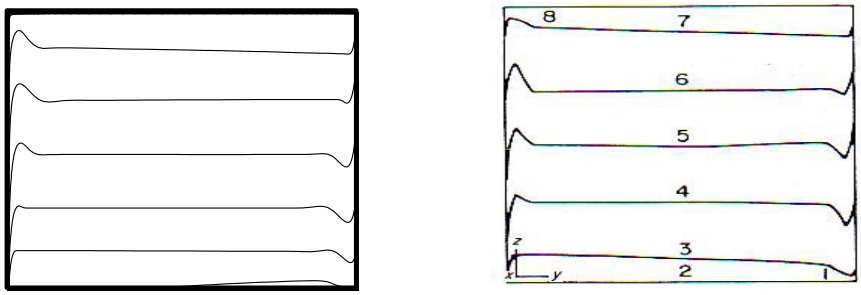

a. present results b. published results[7]

Fig.14 comparison between the present and published results for isotherm contours at Ra=10E12